https://doi.org/10.5194/egusphere-2024-3997
Preprint. Discussion started: 23 January 2025

Comparing thaw probing, electrical resistivity tomography, and airborne lidar to quantify lateral and vertical thaw in rapidly degrading boreal permafrost

Thomas A. Douglas[1], Mark Torre Jorgenson[2], Taylor Sullivan[1], Caiyun Zhang[3]

[1]U.S. Army Cold Regions Research and Engineering Laboratory, Fort Wainwright, Alaska 99703, United States

[2]Alaska Ecoscience, Fairbanks, Alaska 99709, United States

[3]Department of Geosciences, Florida Atlantic University, Boca Raton, Florida 33431, United States

Correspondence to: Thomas A. Douglas (Thomas.a.douglas@usace.army.mil)

Abstract. Permafrost thaw across earth's high latitudes is leading to dramatic changes in vegetation and hydrology. We undertook a two-decade long study on the Tanana Flats near Fairbanks, Alaska to measure permafrost thaw and associated ground surface subsidence via field-based and remote-sensing techniques. Our study focused on four transects that included an unburned area and three fire scars (1988, 2001, and 2010). Three types of permafrost quantification were used. First, repeat measurements of ground-surface elevation and depth to the top of near-surface permafrost were made between 1999 and 2020. Widespread near-surface permafrost degradation was evident between 2004 and 2020 with top-down thaw of near surface permafrost doubling from 18% to 36% over the study period. Multi-year frost and repeat thin permafrost, two types of permafrost aggradation, were almost completely absent by 2020. Second, we calculated rates of top-down versus lateral thaw using airborne lidar measurements collected in 2014 and 2020. Lateral thaw of tabular shaped permafrost boundaries and development of unfrozen zones between the bottom of the seasonally frozen layer and the top of near-surface permafrost (taliks) were evident. Third, repeated electrical resistivity tomography measurements in 2012 and 2020 supported surface-based thaw observations and allowed subsurface mapping of permafrost morphologies up to 20 m deep. The study identified strengths and limitations of the three methods we used to quantify permafrost thaw degradation. Future applications of these methods should apply geospatial analyses to identify variables relating surface and subsurface conditions to project finer scale field-based spatial assessments across broader regions.

1. Introduction

Recent climate warming across high latitudes is leading to permafrost thaw. In interior Alaska this includes top-down thaw of near-surface permafrost (Douglas et al., 2021), formation of unthawed zones (taliks; Farquharson et al., 2022), and lateral expansion of thawed areas (Jorgenson et al., 2020). This permafrost degradation affects hydrology (Marshall et al., 2021), ecological processes (Foster et al., 2019; Mekonnen et al., 2019), the carbon cycle (Douglas et al., 2014) and

https://doi.org/10.5194/egusphere-2024-3997
Preprint. Discussion started: 23 January 2025

infrastructure (Hjort et al., 2022). With warming projected to accelerate over coming decades the spatial extent of permafrost thaw is expected to increase (Wolken et al., 2011).

In warm permafrost regions like interior Alaska surface vegetation and organic matter insulate frozen ground from summer warmth (Shur and Jorgenson, 2007). Removal of this protective cover by wildfire, infrastructure development, and/or climate-driven processes affects the ground thermal regime and leads to accelerated permafrost thaw (Brown et al., 2015; Johnstone et al., 2020; Jorgenson et al., 2022). The relative contributions of press (climate warming) and pulse (fire or infrastructure development) disturbances on permafrost thaw are difficult to quantify over space and time, especially when they are compounded.

Efforts have been made to pinpoint hotspots of permafrost thaw and calculate rates of ground surface subsidence using repeat airborne lidar and other imagery products (Jones et al., 2013; Jorgenson et al., 2022; Zhang et al., 2023). These studies rely on differences in surface elevation or changes in vegetation cover over time to identify where permafrost extent has likely changed in the subsurface. Combining repeat geophysical measurements with surface and subsurface surveys is valuable for mapping three dimensional changes in permafrost extent at mountain (Mewes et al., 2017; Buckel et al., 2022) and lowland sites (Lewkowicz et al., 2011; Douglas et al., 2016; Holloway et al., 2020; Minsley et al., 2023). Comparing ground-based geophysical measurements with airborne remote sensing observations provides the greatest means for quantifying three-dimensional permafrost thaw (Minsley et al., 2015; Uhlemann et al., 2021).

Broad spatial application of terrestrial geophysical measurements with ground truthing is time intensive. As such, great uncertainty remains in our ability to quantify local rates of permafrost thaw linked to ground surface changes that can be remotely sensed over large areas or over time. Increasingly, machine learning geospatial analyses have shown utility in projecting established connections between vegetation and seasonal thaw from the plot (~1 km^2; Zhang et al., 2024) to the regional (~100 km^2; Zhang et al., 2021; 2023; Brodylo et al., 2024) scales. However, these analyses have not been used with high resolution ground surveys or geophysical measurements to measure subsurface permafrost degradation over time.

The focus of this work was to measure three dimensional rates of change in permafrost extent in an area of degrading ice-rich lowland permafrost in interior Alaska. Objectives were to: (1) quantify permafrost degradation from 2012 to 2020 across a range of fire scars (1988, 2001, 2010) and an unburned site using repeat ground-based surveys; (2) use repeat airborne lidar to map thaw stage and calculate the extent, volume, and rates of permafrost loss from vertical versus lateral degradation; and (3) use repeat electrical resistivity tomography to measure changes in subsurface permafrost conditions. This study design allowed us to evaluate the reliability of the three different approaches for quantifying thaw stages.

2 Study site and methods

2.1 Study site climatology, permafrost geomorphology, and fire history

https://doi.org/10.5194/egusphere-2024-3997
Preprint. Discussion started: 23 January 2025

Our study focused on four transects located along the northern edge of Tanana Flats, a lowland underlain by discontinuous permafrost south of Fairbanks, Alaska (Fig. 1). Covering approximately 6,000 km^2, Tanana Flats is a broad valley filled with fluvial and glaciofluvial sediments spreading northward from the Alaska Range to the Tanana River. The area is characterized by a heterogeneous patchwork of forested areas underlain by discontinuous permafrost up to 50 m thick (Chacho et al., 1995). Numerous bogs and fens dot the landscape. They are not generally underlain by permafrost but their outside margins are delineated by frozen ground (Douglas et al., 2016). From the air these wetland features are readily apparent, however, the morphology of their subsurface permafrost boundaries, particularly along their margins, is not well known. More detailed descriptions of the ecology, hydrogeology, and permafrost thermal state of our sites are provided elsewhere (Brown et al., 2015; Douglas et al., 2016; Lara et al., 2016; Jorgenson et al., 2022).

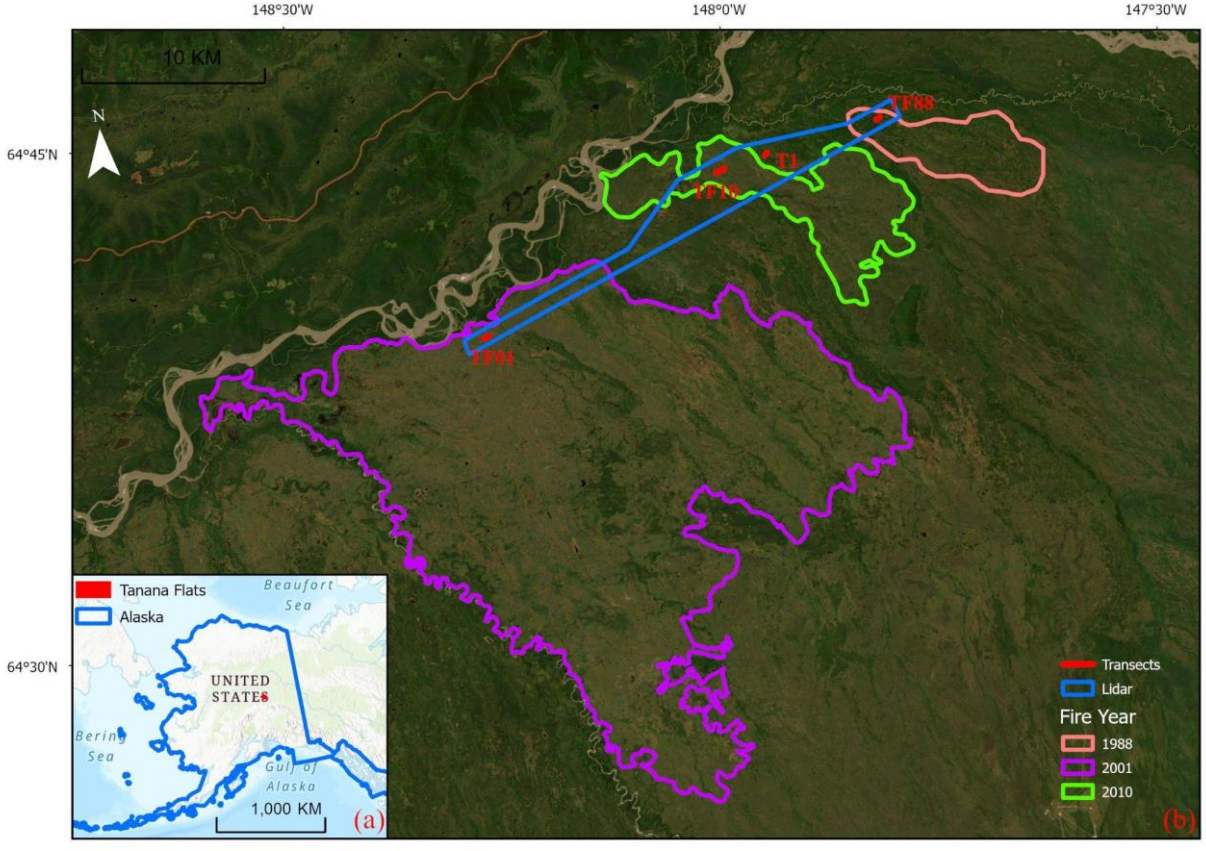

Figure 1. Study area in interior Alaska (a) identifying the regional location in Alaska and (b) the location of four transects: T1 (unburned), TF88 (burned in 1988), TF01 (burned in 2001), and TF10 (burned in 2010). Perimeters for the 1988, 2001, and 2010 fires are also provided. Imagery from 8/26/2024 WorldView 3 acquisition provided by Maxar Technologies (Palo Alto, California).

https://doi.org/10.5194/egusphere-2024-3997
Preprint. Discussion started: 23 January 2025

The regional climate is continental with a mean annual temperature of -2.4 °C and mean monthly temperatures ranging from 16 °C in summer to -22 °C in winter. Annual extremes range from -51 °C to 29 °C (Jorgenson et al., 2020). Typical mean annual precipitation is 28 cm water equivalent with 45% of this as snow (Liston and Hiemstra, 2011). Based on decadal mean annual temperatures the area warmed ~2.3 °C between the 1930s-1940s and 2010-2020. Over that same timeframe mean summer temperatures (May 1 to October 10) warmed ~1.7 °C while mean winter temperatures (October 11-April 30) warmed 2-4 °C (Douglas et al., in press).

The dominant forest cover includes deciduous Alaska paper birch (*Betula neoalaskana*) and aspen (*Populus tremuloides*) mixed with pure or mixed white spruce (*Picea glauca*). Ground cover is dominated by *Sphagnum* spp. In poorly drained areas feather mosses (*Pleurozium schreberi*, *Hylocomnium splendens*) are common. This land cover is well suited to protect permafrost from warm summers, however, it is also subjected to regular intervals of wildfire (Douglas et al., 2014; Brown et al., 2015; Potter and Hugny, 2020).

The Tanana Flats lowland has experienced numerous wildfires and we established transects to represent high severity fires in the summers of 1988 (TF88, 64.734 °N, 147.826 °W), 2001 (TF01, 64.644 °N, 148.295 °W), and 2010 (TF10, 64.716 °N, 148.010 °W). Transects were established in 2011 as part of study to assess the effects of fire on permafrost (Nossov et al., 2013): TF88 (200 m) is in an area burned in ~1950 that reburned in 1988; TF01 (initially 100 m in 2011, extended to 320 m in 2012) is in an area burned in 2001, and TF10 (initially 100 m in 2011, extended to 200 m in 2012) is in an area burned in 2010. Transects were positioned to cross a range of permafrost and non-permafrost ecotypes. We also included an unburned site (T1, 64.722 °N, 147.959 °W) that has not burned in recent years (~1950s-present) for comparison. T1 (initially 100 m in 1999, extended to 200 m in 2012) was established during ecological land surveys (Jorgenson et al. 1999). In Douglas et al. (2016) T1 is referred to as "1930" and TF50 is referred to as "1988".

2.2. Data collection, processing, and analysis

2.2.1 Field sampling design and measurements

Along our four transects we measured surface topography, seasonal thaw depth, areal extent and depth of standing water, and electrical resistivity tomography (ERT) in the fall of 2012. Sites were revisited almost yearly until 2020 to repeat measurements of ground-surface elevation, thaw depths, and water depth, and to download temperature loggers. ERT lines and elevation surveys were remeasured in 2020.

Repeated thaw probing using a metal rod in late summer quantified changes in the top of near-surface permafrost. Maximum probing depths varied from 2.5 to 4.0 m depending on the number of extensions used, occurrence of gravel, and stickiness of unfrozen silts. We differentiated three quasi-stable permafrost conditions and five degradation stages. For permafrost types, undegraded (UD) was assigned when thaw depths were less than 0.8 m (typical maximum range of late summer thaw for organic-rich soil). We considered this "stable" permafrost. Multi-year frost (MF) was thin frost (typically

https://doi.org/10.5194/egusphere-2024-3997
Preprint. Discussion started: 23 January 2025

10-30 cm thick as detected by probing through the frozen layer) that persisted for one to several years. New repeat permafrost (NPR) had a frozen layer from 1 to several meters thick (detected through coring) that formed in old thermokarst bogs and persisted for decades or more. For degradation stages, degradation-initial (DI) occurred where thaw depths increased over time to ~1.1 m depths. Degradation-progressive-shallow (DPS) was assigned when the permafrost surface was detected below 1.1 m indicating development of an open talik (unfrozen zone between seasonal frost and permafrost). Degradation-progressive-deep (DPD) identified permafrost that retreated below probing depth. We grouped these three into a broader category of vertical degradation that we considered "unstable" permafrost. Degradation-lateral (DL) was used where permafrost thawed along margins of permafrost plateaus; these areas quickly joined "through" taliks (thawed zone penetrating all the way through permafrost) of adjacent old thermokarst bogs or fens. Degradation-complete-old (DCO) or "old thaw" was assigned to locations within old thermokarst bogs and fens where permafrost was not detected within probing depth and where we assumed a through talik had developed.

To independently estimate top-down and lateral permafrost thaw based on repeat thaw probing we stratified each transect into three zones: (1) "old thaw" which were completely thawed in 2012 that we associated with thermokarst bogs and fens; (2) "lateral thaw" where permafrost thawed along margins of permafrost plateaus between 2012 and 2020 with thaw extending below probing depth (2.5-4.0 m depending on rod extensions and occurrence of gravel); and (3) "vertical thaw" of top-down permafrost where near-surface permafrost was detected with the 3 m probe.

Within vertical thaw zones we further differentiated two surface conditions useful for assessing ERT measurements. First, "stable" permafrost where thaw depths were always less than 0.8 m, typically within the range of annual variability, in organic-rich, fine-grained soils. Second, "unstable" permafrost where thaw depths exceeded the normal range or where an unfrozen region (open talik) developed from 2012 to 2020 between the bottom of the active layer and the top of near-surface permafrost.

For ERT measurements we used an Advanced Geosciences Incorporated (Austin, Texas) SuperSting R8 eight-channel portable meter with 84 electrodes at 2 m spacing for transects T1, TF88, and TF01 and 1-m spacing for transect TF10. Electrodes ranged from 0.45 m to 1 m in length. More detailed operational information for measurements made in 2012 is provided in Douglas et al. (2016). A dipole-dipole measurement geometry was used for all ERT surveys due to its sensitivity to lateral features and our focus on changes in near-surface permafrost distribution.

ERT survey data were processed with the R2 family of codes using open-source ResIPy (Blanchy et al., 2020) software to remove noisy data points (i.e. resistivity values with noise greater than 3%) and find inverse model solutions using least-squares inversion methods (Loke and Barker, 1996; Loke et al., 2003). Approximating resistivity differences between 2012 and 2020 measurements was achieved by projecting 2020 resistivity measurements onto the 2012 inversion mesh and calculating the log difference within each mesh element relative to the 2012 inverse model solution according to:

$$\Delta\Omega m_{2012-2020} = log(\Omega m_{2012}) - log(\Omega m_{2020}).$$

https://doi.org/10.5194/egusphere-2024-3997
Preprint. Discussion started: 23 January 2025

Here, $\Delta\Omega m_{2012-2020}$ represents the log difference in inverse model solutions between 2012 and 2020 field campaigns. We acknowledge topographic differencing errors from performing an inversion of 2020 resistivity data on the 2012 inversion mesh and incorporate differencing errors into our final interpretations and discussion of uncertainty in the following sections.

2.2.2 Airborne lidar data acquisition and analysis

Airborne lidar surveys were conducted by Quantum Spatial Incorporated (Anchorage, Alaska) in May 2014 and 2020 in a period of 95% snowmelt with leaf-off conditions using a Lecia ALS laser system, leading to an average pulse density larger than 25 points/m^2 over the targeted area (~40 km^2, Figure 1) where our field transects were located. From the high density lidar point cloud data, the vendor applied a hydro-flattening procedure to eliminate artifacts in the digital terrain caused by both increased variability in ranges or dropouts in laser returns due to the low reflectivity of water and generated a 0.25-m lidar DEM products. A total of 183 Ground Control Points (GCPs) were measured using real time kinematic and post processed kinematic techniques to validate the accuracy of the lidar products. A Root Mean Square Error (RSME) less than 9.2 cm was reported in terms of these GCPs. More details about lidar data acquisition and processing can be found in Douglas et al. (2016). . From the DEM products, we extracted lidar DEMs and calculated the elevation difference between 2014 and 2020 in a 300 m by 500 m buffer strip encompassing each transect to map thaw degradation stages and quantify thaw extent and volumetric loss within the buffered transect areas.

From repeat lidar DEMs and corresponding elevation changes we mapped the three thaw degradation types along each transect to be consistent with our field stratified zones: (1) old thaw as areas that had minimal elevation change within the thermokarst bogs and fens which often had a low elevation within a landscape; (2) lateral thaw as areas adjacent to old thaw areas that collapsed to the same elevation as the old thaw areas and had a larger elevation change; and (3) vertical thaw areas as the remaining terrain and often found at permafrost plateaus covered by trees.

We identified elevation change and DEM thresholds for each zone based on field measurements which were then applied to map thaw degradation stages to quantify top-down thaw, lateral thaw, and corresponding volumetric changes for each buffered transect using repeat lidar DEMs. To map thaw degradation stages, we applied an object-based analysis approach in which a multiresolution segmentation was used to segment the lidar DEM difference image first, and then the mean DEM of 2014 and 2020 and the DEM difference were calculated. This object-based analysis approach reduces “salt-and-pepper” effects. Thaw extent and volumetric loss from lateral and vertical thaw were then calculated based on corresponding area and elevation changes for each object and summarized for each buffered transect.

https://doi.org/10.5194/egusphere-2024-3997
Preprint. Discussion started: 23 January 2025

3 Results

3.1 Degradation stages identified along the transects

We compiled the repeat surveys of surface topography, water depths, thaw depths, and ancillary subsurface measurements from the four transects to define trends of subsurface thaw and corresponding ground surface settlement between 2012 and 2020 (Figs. 2 and 3). We differentiated trends across each transect into six degradation stages. UD were areas where thaw depths remained <100 cm and annual changes were <30 cm. They occurred along 29% of the transects in 2012 and decreased to 8% by 2020 (Figs. 2 and 3). DI were regions where thaw depths were >100 cm and <120 cm or had increased by >30 cm over time as a brief transitional stage before further degradation. They occurred along 36% of the transects. DPS indicates where vertically increasing thaw depths were >120 cm and still within probing depth (typically 250-300 cm), increased from 12% to 20% between 2012 and 2020. DPD represented regions where thaw depths increased to beyond probing depth and they increased from 6 to 16%. Together, the shallow and deep progressive degradation (i.e. top-down thaw of near surface permafrost) increased from 18% to 36% over the 8 year study period. The DPD stage denotes areas where thaw has progressed below our thaw probing depths and are presumed to still represent open taliks. DL, where permafrost thawed laterally along the margins of bogs and fens, increased slightly from 3% to 6%. Regions characterized as DCO occurred under old bogs and fens and presumably had completed degradation through the entire permafrost zone to form through taliks. They increased slightly between 2012 and 2020 from 35% to 44%. We attribute this change, however, primarily due to the loss of Repeat-Permafrost-Thin (RPT) and MF (Figs. 2 and 3) near the surface. MF was used to differentiate areas with a thin layer (typically <30 cm) of frozen ground that persisted for 14 years (permafrost is conventionally defined as frost persisting more than 2 years). MF decreased from 7% to 0%.

https://doi.org/10.5194/egusphere-2024-3997
Preprint. Discussion started: 23 January 2025

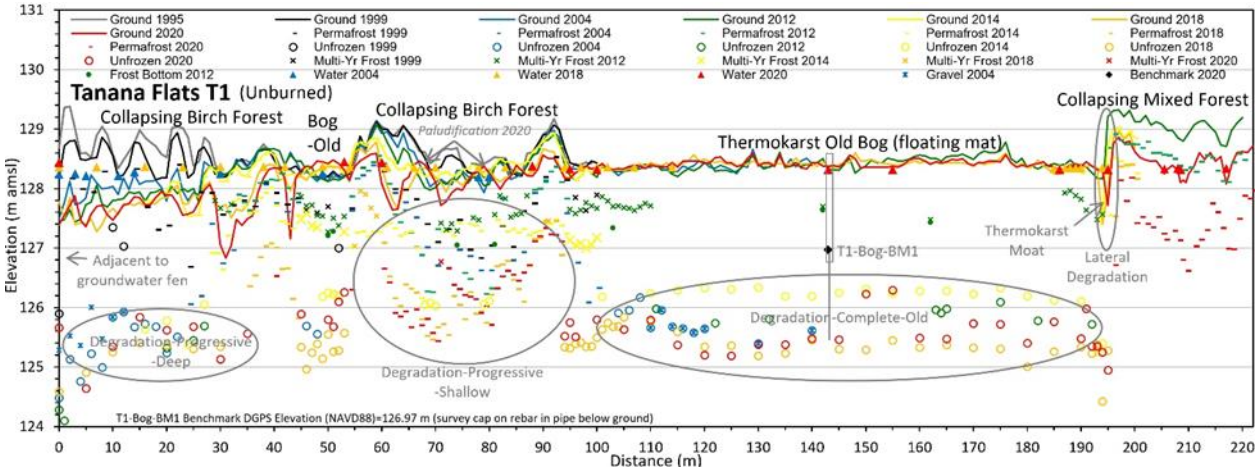

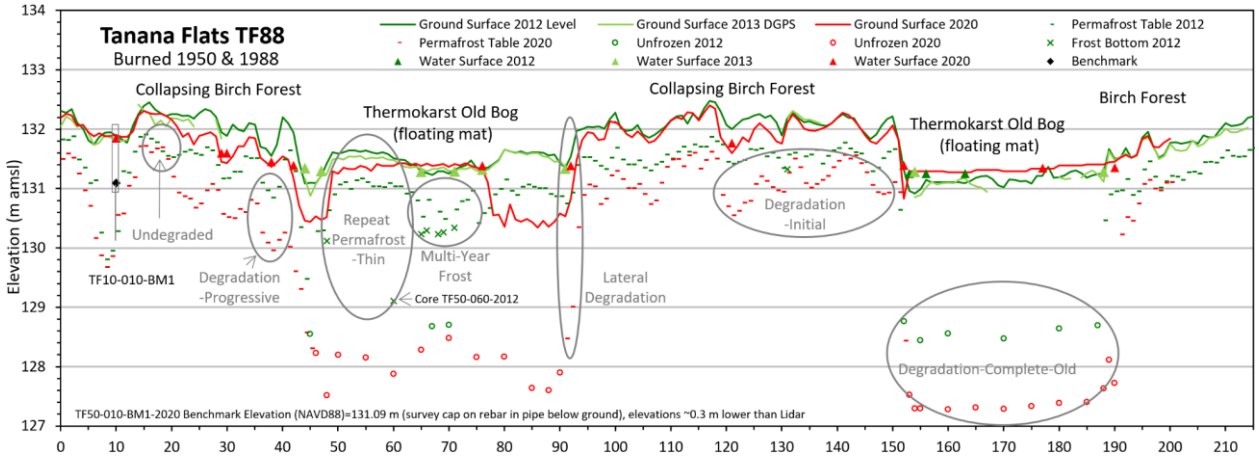

Figure 2. Topo-profile for T1 (top) and TF88 (bottom) showing elevations of the ground surface, water surface, permafrost table, and maximum-observed unfrozen depths from 1999 to 2020. Also shown are representative transect segments in varying stages of permafrost degradation and aggradation.

https://doi.org/10.5194/egusphere-2024-3997
Preprint. Discussion started: 23 January 2025

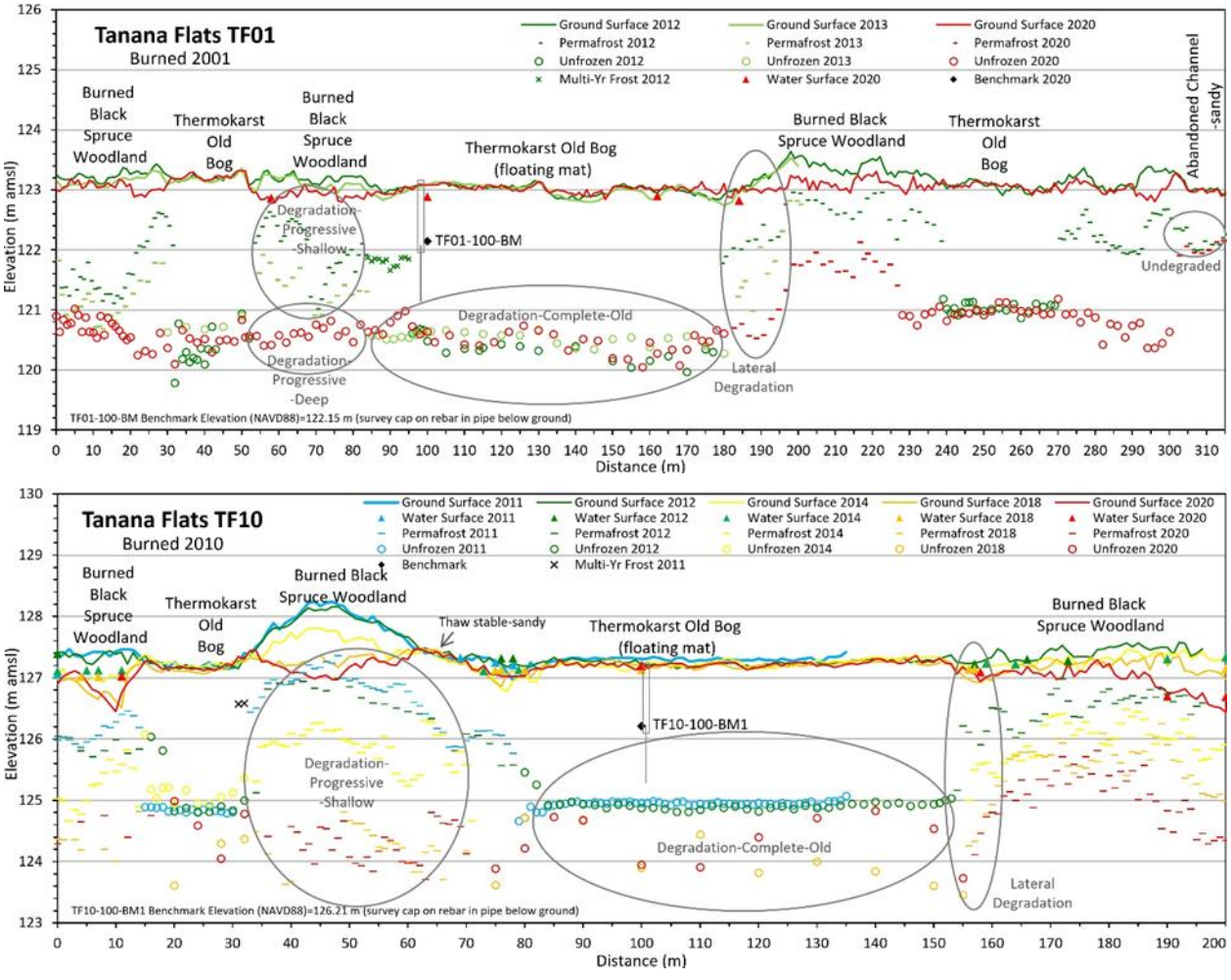

Figure 3. Topo-profile for TF01 (top) and TF10 (bottom) showing elevations of the ground surface, water surface, permafrost table, and maximum-observed unfrozen depths from 2011 to 2020. Also shown are representative transect segments in varying stages of permafrost degradation and aggradation.

Overall, degradation changes were mostly minor from 2012 to 2014 but exhibited large changes by 2020 (Fig. 4). We highlighted differences in degradation stages across the four transects using observations along the first 200 m where measurements were consistently taken over time. Trends were highly variable among transects in response to differences in soil texture, ground-ice content, surface organics, old thermokarst history, and fire history.

https://doi.org/10.5194/egusphere-2024-3997
Preprint. Discussion started: 23 January 2025

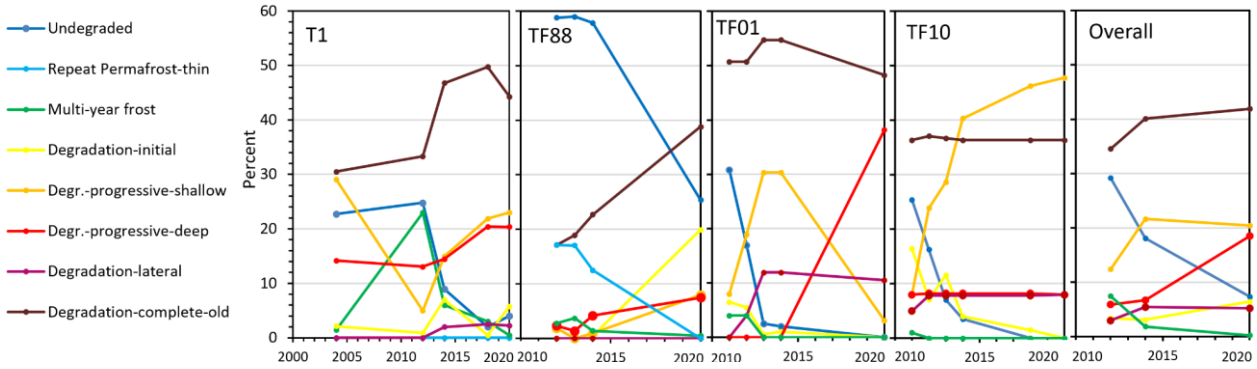

Figure 4. Trends in extent (percent of transect) of the eight degradation/aggradation stages at four transects (0-200 m) over time.

UD showed steep losses across all transects (0-200 m), and was eliminated at TF01 and TF10. TF88 had the highest initial percentage (59%), which persisted from 2012 to 2014, but then dropped to 27% by 2020. The more recently burned TF01 and TF10 had the steepest losses during 2012-2014. DI showed a substantial increase at TF88 by 2020 (20%) and a substantial decrease at TF10 as the stage transitioned to DPS.

Degradation-progressive, both shallow (DPS) and deep (DPD), fluctuated substantially across the four sites, in large part due to the transition of the shallow phase into the deep phase. TF10 was the only transect to show a large, consistent increase in DPS (from 8% to 48%). DPD showed a large increase at TF01 (38%), small increases along T1 and TF88 (7%), and no change at TF10. We attribute the large increase in DPS at TF10 to the short-term response to the 2010 fire and the large increase in DPD at TF10 to a longer-term response to the 2001 fire.

DCO was abundant across all transects; it held fairly steady at TF01 and TF88 but showed large increases at T1 and TF88 due to the loss of RPT and MF near the surface above the unfrozen zone at depth. RPT was used to differentiate young bodies of permafrost formed in response to ecological succession and periods of extremely cold and dry winters (Jorgenson et al. 2020). RPT occurred only within an old bog at TF88 (Figs. 2 and 3) and was measured to be 193 cm deep based on core TF88-060-2012. We estimated it formed during extremely cold winters in the 1960s; it was last observed in 2014 and disappeared by 2020. MF was evident at all transects during 2012-2014 and had completely disappeared by 2020. MF was most prevalent at T1 (23%) near the surface of the old thermokarst bog. When this thawed the segments reverted to DCO. At the other transects, MF covered less than 4%.

3.2 Thaw settlement revealed from field measured topographic data

Thaw settlement varied nearly ten-fold across degradation stages and transects based on differences in relative ground heights of degradation stages in 2020 relative to UD in 2012 (Figs. 2 and 3). Overall, mean thaw settlement was deepest for DL compared to other stages at TF01 and TF88 while DPD was deepest at T1 and DPS was deepest at TF10. DL was 918 cm

https://doi.org/10.5194/egusphere-2024-3997
Preprint. Discussion started: 23 January 2025

deeper than DCO, indicating that over time accumulation of post-thermokarst peat raised the ground surface. Overall, thaw settlement across all stages tended to be deepest at TF88 and T1, and shallowest at TF01 and TF10. We attribute the high variability to differences in soil properties, ground ice contents, and the timing of degradation onset.

The ratio of increased ground surface thaw settlement to thaw depth (Fig. 5) directly relates to excess ice content. For example, a ratio of 0.38 indicates an average excess ice volumetric content of 38% in the permafrost profile before thawing. Overall, the relationship was moderately strong (R^2=0.61, n=239), but varied slightly among transects (R^2 ranged from 0.51 to 0.70). The ratio increased nearly three-fold between 2012 and 2020 between TF01 (0.23 regression slope coefficient) to T1 (0.63). The overall ratio for all measurements was 0.38. Scatter in the relationship indicates substantial variability which we attribute to differences in soil characteristics and surface conditions. For example, high thaw depths with negligible settlement occurred in sandy soils along TF10. Floating mats along laterally collapsing margin also were a problem, especially along TF88 where floating mats developed over time raising the surface even while thaw depths continued to increase. Without this influence, the relationships would have been stronger and the ratio would be larger.

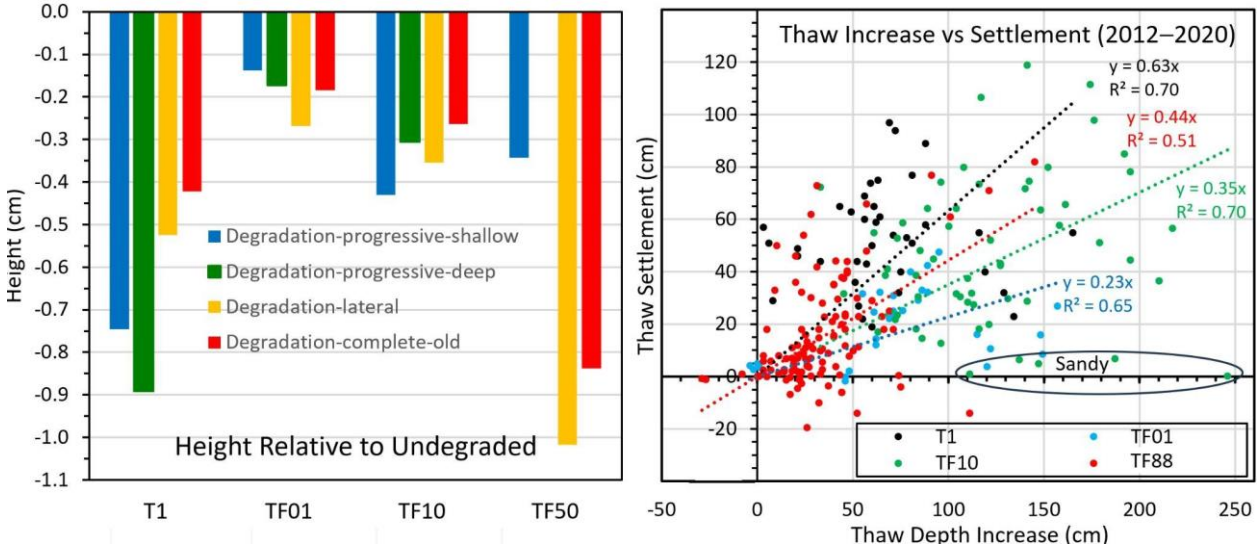

Figure 5. Change in elevation (cm) of mean surface heights in 2020 by degradation stage relative to mean undegraded height in 2012 (left), and relationship of increased thaw settlement to increased thaw depth from 2012 to 2020 by transect (right). Note that surface elevation of degradation-complete-old includes new peat (floating mat) added after thermokarst and thus does not represent total settlement of the original surface.

3.3. Mapping thaw degradation stages from repeat lidar

Maps of lidar DEM differences between 2014 and 2020 (Fig. 6) show ground surface elevation changes over the 6 year period. In our transect surveys we did not identify any areas that rose in elevation over time so we attribute increases in

https://doi.org/10.5194/egusphere-2024-3997
Preprint. Discussion started: 23 January 2025

255 elevation (positive values in Fig. 6) to higher vegetation or higher water levels in 2020. Lateral thaw into the permafrost plateau is evident at all four sites. TF10 shows the greatest subsidence of the plateaus themselves.

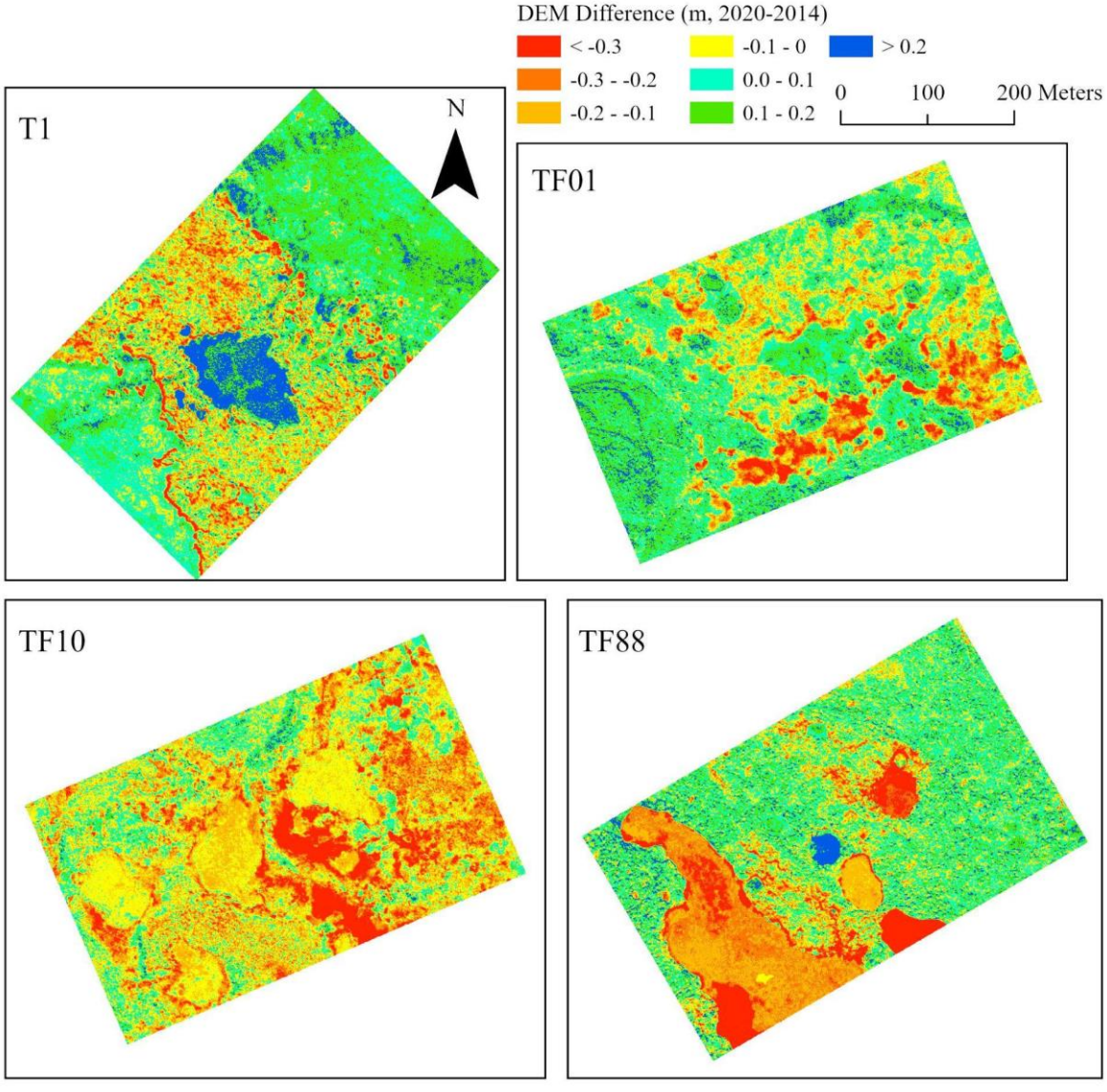

Figure 6. Lidar DEM differences between 2014 and 2020 across 300 m by 500 m regions surrounding each of the four transects.

260 To map our three defined thaw degradation zones (old thaw, lateral thaw, and vertical thaw) elevation thresholds in 2014 and thresholds of elevation change between 2014 and 2020 were identified from the field surveyed ground elevation, thaw depth data, and other ancillary data we collected along each transect. For the unburned site T1 old thaw was found at fens and

https://doi.org/10.5194/egusphere-2024-3997
Preprint. Discussion started: 23 January 2025

bogs with elevation less than 128.24 m and an elevation change less than 0.1 m. For TF01, the identified elevation threshold was 123.23 m in 2014 and the elevation difference threshold was 0.15 m; for TF10, an old thaw was found at elevation less than 127.49 m with elevation change less than 0.15 m; for TF88, old thaw was found at elevation less than 131.79 m with elevation change less than 0.1 m. Based on these thresholds, old thaw areas were objects with an elevation in 2014 less than the identified threshold and elevation change less than the threshold 0.1 m for T1 and TF88 and 0.15 for TF01 and TF10. Once the objects with old thaw were identified, these objects were spatially dissolved, and adjacent unidentified objects would be the potential objects as lateral thaw. These adjacent objects were further refined and finalized as lateral thaw areas if they had larger elevation change due to ground surface collapse (larger than the threshold). The remaining objects were labeled as vertical thaw.

Figure 7 shows thaw degradation zones classified by these rules. The maps delineate well the thaw extent and stages for old thaw found over bogs and fens (in green) where DCO was observed. Lateral thaw degradation (in blue) is evident along the edges of bogs and fens. Vertical thaw (in red) over high elevation permafrost plateau areas denotes where top-down thaw occurred due to climate warming or fire disturbance.

https://doi.org/10.5194/egusphere-2024-3997
Preprint. Discussion started: 23 January 2025

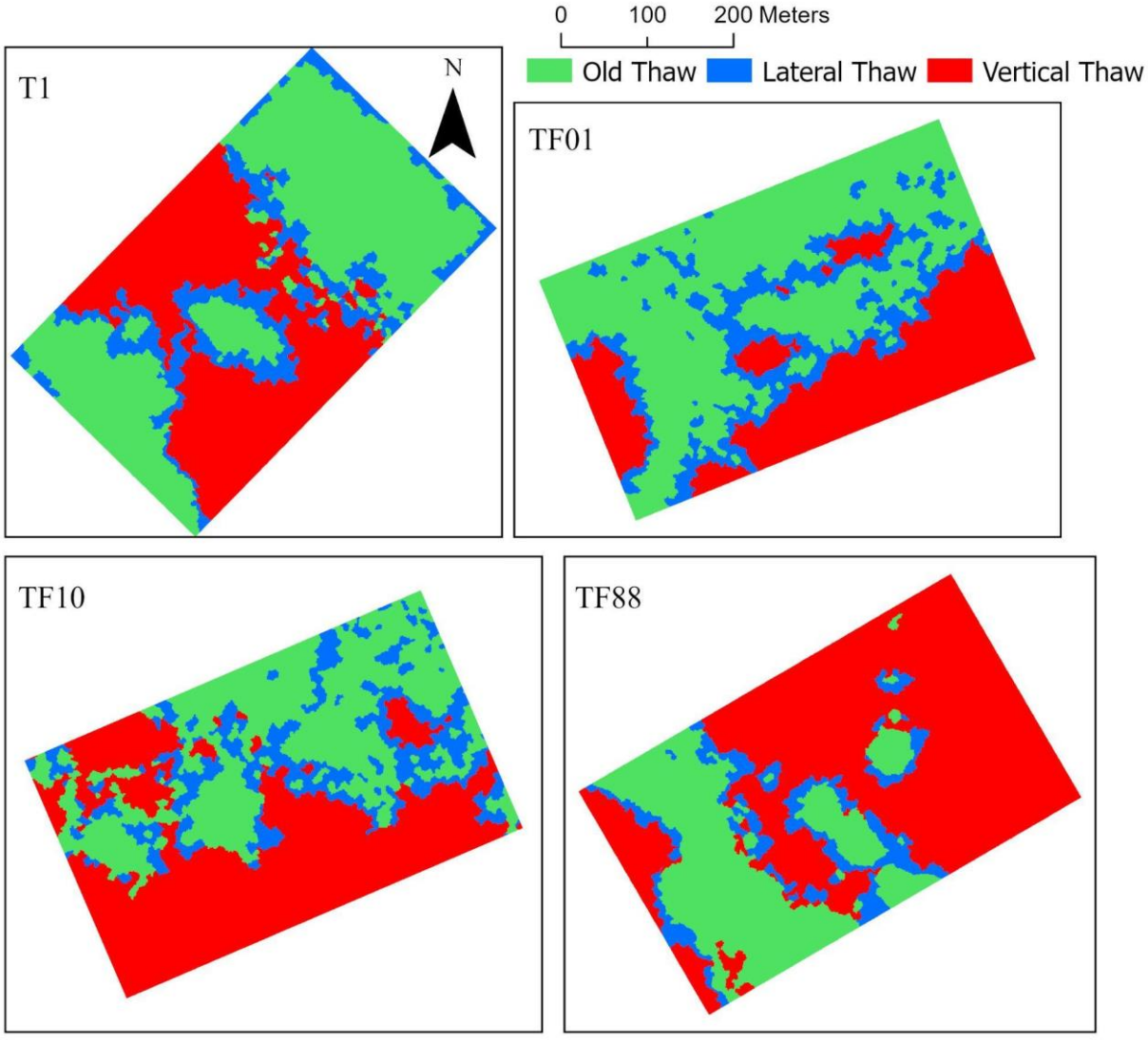

Figure 7. Lidar detected thaw degradation stages across 300 m by 500 m regions surrounding each of the four transects between 2014 and 2020.

280 The estimated thaw extent and volumetric loss from lateral and vertical thaw for each buffered transect is displayed in Fig. 8 and summarized in Supplemental Table 1. TF10, the 2010 fire scar, had the largest lateral thaw of 26,555 m^2 (17.7%) and corresponding volumetric loss of 5,015 m^3. Its vertical thaw was also relatively high with an extent of 69,125 m^2 (46.1%),

https://doi.org/10.5194/egusphere-2024-3997
Preprint. Discussion started: 23 January 2025

leading to the largest volumetric loss of 9,755 m^3 among all transects. The largest extent of vertical thaw was observed at TF88 (91, 206 m^2, 60.8%) but the volumetric loss due to vertical thaw was moderate (3, 350 m^3).

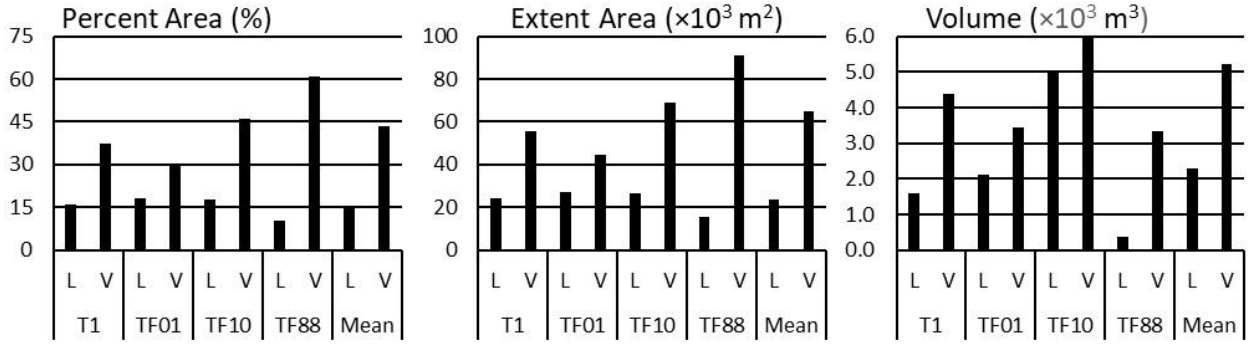

Figure 8. Thaw extent (percent area and m^2) and volumetric settlement loss (m^3) due to lateral (L) and vertical (V) thaw derived from repeat lidar DEMs for a 300 m by 500 m buffered area around each transect.

3.4. Electrical resistivity tomography measurements

ERT measurements were made across the transects in 2012 and 2020. Details from the 2012 collection and relationships between fire disturbance and permafrost degradation along the transects between 2012 and 2014 are presented in Douglas et al. (2016). Similar operating conditions were repeated for the 2020 collection (Fig. 9). This allowed us to quantify the percent change in resistivity values at depths up to 20 m over the eight years of elapsed time.

Resistivity values greater than 600-800 Ωm (log_{10} resistivity values of 2.8-2.9) have been found to correlate with syngenetic permafrost in the greater Fairbanks region (Hoekstra and McNeill, 1973; Douglas et al., 2008). As such, values above this are generally associated with frozen ground. Values below log_{10} resistivity of 2.8 Ωm are considered absent of permafrost and we interpret those areas as unfrozen. In both 2012 and 2020 the major unfrozen zones and permafrost plateaus are readily apparent from their higher resistivity values and low active layer depths. Resistivity values decreased between 2012 and 2014 and these correspond with the thaw degradation stages identified earlier.

All transects had areas exhibiting decreases in resistivity values and associated ground surface subsidence over the eight year study period indicating top-down thaw. TF10, the transect representing the most recent wildfire, yielded the greatest values for top-down thaw (up to 3 m) and associated subsidence (~1 m). Permafrost plateaus present at TF01 (-20 to 25 m and 50 to 95 m) and TF10 (0 to 20 m; 40 to 80 m) in 2012 experienced major subsidence by 2020. Permafrost plateaus at TF88 (50 to 70 m; 125 to 180 m) also showed thaw subsidence by 2020. The site with the second greatest top-down thaw values (~ 2 m) was the second most recent fire (TF01). Thawed areas correspond with large percent decreases in resistivity values over time.

https://doi.org/10.5194/egusphere-2024-3997
Preprint. Discussion started: 23 January 2025

We measured the difference in resistivity values model solutions between 2012 and 2020 measurements (Fig. 9).In interior Alaska resistivity values above 600-800 Ωm (log_{10} resistivity values of 2.8 to 2.9 Ωm) correlate with conductive permafrost material (Hoekstra and McNeill, 1973; Douglas et al., 2008; 2016; Minsley et al., 2022). The top of near-surface permafrost corresponds with sudden decreases in log_{10} resistivity from values greater than 2.5 Ωm above the permafrost (active layer) to values between 3 and 4 Ωm where permafrost is present. Old thermokarst bogs are readily identified by low resistivity values and permafrost plateaus have rapid vertical changes in resistivity over the upper ~3 m that are confirmed as permafrost by thaw probing. Resistivity values decreased between 2012 and 2020 for every measurement location across all transects at depths of up to ~20 m. Top-down thaw of permafrost plateaus and lateral thaw along bog margins is evident. The difference map between the two resistivity campaigns shows the greatest decreases in resistivity occurred in permafrost plateaus and this supports surface surveys along the transects (Figs. 2 and 3).

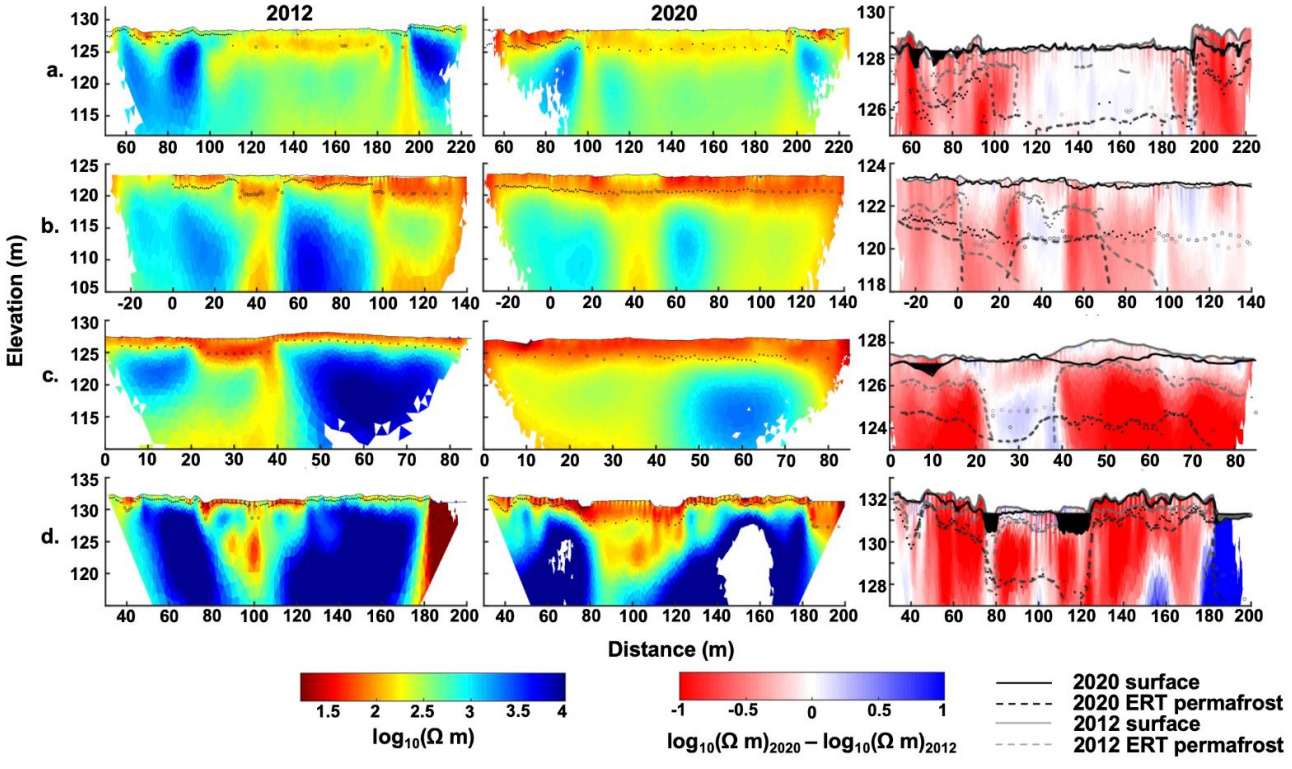

Figure 9. Repeat ERT data for (a) T1, (b) TF01, (c) TF10, (d) TF88. Left (2012) and middle (2020) show thaw depth (dots), maximum observed unfrozen depth (open circles), and surface water (triangles) atop inverse model results. The right column shows the log difference between 2012 and 2020 plotted on the 2012 inversion mesh. Black and gray lines represent the surface topography and permafrost boundary as interpreted from dipole-dipole ERT surveys and thaw probe measurements.

https://doi.org/10.5194/egusphere-2024-3997
Preprint. Discussion started: 23 January 2025

4. Discussion

Interior Alaska permafrost has been slowly thawing for the past ~500 years with sporadic periods of accelerated thaw typically attributed to wildfire and subsequent permafrost stabilization or aggradation associated with forest succession (Jorgenson et al. 2001; Jones et al., 2013). Air temperature increases since the 1970s have led to increased permafrost temperatures and widespread thaw (Osterkamp, 2005). Numerous recent studies show an acceleration of permafrost degradation with deeper seasonal thaw depths (Douglas et al., 2020; Euskirchen et al., 2024), widespread talik expansion (Farquharson et al., 2022), and an increased prevalence of thermokarst feature development (Douglas et al., 2021; Minsley et al., 2022; Brodylo et al., 2024).

All four of our transects contain low lying old thermokarst bogs surrounded by permafrost plateaus consisting of mixed forest, birch forest, or black spruce woodland (Figs. 2 and 3). These are the most common landforms above boreal discontinuous permafrost. At T1, an unburned site, the top of near-surface permafrost below the collapsing birch forest increased steadily from ~0.5 m in 1999 to ~2 m in 2020. TF88, which burned in 1950 and 1988, also shows top-down thaw associated with areas of collapsing birch forest but not as much subsidence (~0.5-1 m) associated with this thaw as T1. This is likely due to lower ice content lenticular ice from 1.2 to 2.8 m depth at TF88 compared to braided ice from 1.5 to 2 m at T1 (Brown et al., 2015). TF01, a fire scar from 2001 dominated by burned black spruce, was already showing signs of top-down thaw. For example, the top of near-surface permafrost was ~2 m deep in 2011 and it increased to >3 m at some locations during our decade of study. However, subsidence associated with this thaw was lower than at other transects, likely due to the lowest ice contents in the upper 3 m of any of the four sites (Brown et al., 2015). Permafrost warming and related top-down and lateral thaw continued between 2012 and 2020. TF10, the most recent fire scar, had the highest rates of top-down thaw (>2 m) and related surface subsidence (up to 1.2 m) of any site. These results support numerous studies showing that the first decade following a wildfire is typically associated with the most rapid surface warming and that permafrost thaw slows after vegetation starts to recover (Gibson et al., 2018; Holloway et al., 2020). We used results from repeated thaw probe measurements, ERT, and airborne Lidar to assess their relative strengths and weaknesses for quantifying changes in ecosystem-driven discontinuous permafrost in a boreal ecosystem. More detail is provided in the next section.

4.1 Relative Strengths and Weaknesses of different permafrost degradation measurements

4.1.1 Repeat thaw probing and ground surveys

Thaw probing, accompanied by surveying of ground and water-surface elevations, had the advantage of precise measurements of changes in the permafrost table that are useful for categorizing degradation stages (Figs. 2 and 3). Probing can detect marked changes in soil texture (peat, silt, sand, gravel) with depth. It is important to note the importance of measuring both thaw depth and thaw settlement, which allows calculation of ice content and accurate measurement of the

https://doi.org/10.5194/egusphere-2024-3997
Preprint. Discussion started: 23 January 2025

change in the elevation of near-surface permafrost. Ice content measurements, where available, can be used to compare to the estimated ice contents.

For the most part the top of near-surface permafrost measured from frost probing (< 3 m) matches the presence of permafrost inferred from sudden increases in resistivity to values ~2.8 Ωm. At all sites the margins between bog features and permafrost plateaus degraded laterally during the study period. Douglas et al. (2016) showed irregular margins along the edges of the permafrost bodies at the four transects. Tabular "shelves" were evident in ERT measurements, particularly at T1 ("1930" in the earlier study), TF01, and TF10. Other studies of permafrost thaw and thermokarst development in peatlands have shown lateral thaw degradation created thermal "niches" of higher subsurface thaw rates underneath "shelves" (Jorgenson et al., 2012; O'Donnell et al., 2012). These features can lead to thaw probe measurements of near-surface permafrost and aerial photo imagery of landforms associated with permafrost where tabular permafrost areas are only a meter or two thick. As such, it is likely the amount of permafrost is overestimated in these areas. Our repeated geophysical and thaw probe measurements show these tabular bodies can thaw completely in just 8 years. It likely takes longer for vegetation to respond to the changes in ground surface conditions associated with permafrost loss, for example, for trees to get waterlogged and die and for vegetation associated with standing water to colonize those areas.

The large disadvantage of probing is that it is limited to the top 2-3 m of fine-grained soils and determining frost boundaries becomes more uncertain (10 to 30 cm error) as unfrozen water contents increase during partial permafrost thaw. At depths greater than 3 m, determination of penetration refusal due to frost becomes less reliable due to friction along the probe. Also, the occurrence of sand and gravel at depth impedes probing. Borehole logging of soils can reduce some of these uncertainties.

4.1.2 Repeat airborne lidar

Repeat Lidar (Figs. 6 and 7) provides high-precision measurements of surface-elevation change, and can be used to model vertical versus lateral thaw (thaw along changing permafrost margins) at large areal extents. Collections in 2014 and 2020 showed that almost every permafrost plateau margin shrunk as lateral thaw expanded old thermokarst bogs into plateaus. All of the plateaus exhibited vertical (top-down) thaw of near-surface permafrost. No areas at any of our buffered transects exhibited signs of permafrost aggradation or increases in ground surface elevations that are not attributable to higher vegetation or elevated water levels in 2020 compared to 2014.

Since the transects contain different aerial extents of old thermokarst bog and permafrost plateau terrains we cannot compare the percentage of lateral and vertical thaw across the transects (Supplemental Table 1). However, in all four buffered transect areas vertical thaw extents and volumetric loss were greater than lateral thaw. The most recent fire scars (TF01 and TF10) yielded the greatest rates of vertical and lateral thaw extent and volume loss. TF10 exhibited more than twice the amount of thaw as TF01 and this supports ground surface measurements showing the greatest thaw subsidence across transect TF10 (Fig. 3). As stated earlier, differences in rates and volumes of vertical and lateral thaw at a given transect are likely attributable to the different ice contents of the near-surface permafrost that thawed.

https://doi.org/10.5194/egusphere-2024-3997
Preprint. Discussion started: 23 January 2025

Changes in surface water conditions, vegetation growth, and floating soil mats in thermokarst features affect Lidar surface elevation measurements. Also, airborne lidar does not provide information about below ground soil or permafrost characteristics. We used settlement of >0.3 m as the threshold for detecting significant permafrost thaw, but it is notable that substantial areas of old thermokarst bogs and fens also had water-level changes greater than that. Thus, repeat airborne lidar is more reliable in ice-rich areas (T1 and TF88) than ice-poor ones (TF01 and TF10). In addition, lidar can detect permafrost thaw only where the ground surface remains above water. If the original ground surface settles below the water level or precipitation increases markedly from one acquisition to the other, thaw settlement can be masked.

4.1.3 Repeat Electrical resistivity tomography

Repeat ERT (Fig. 9) has a strong advantage in delineating permafrost boundaries down to depths of 20 m or more, and is particularly useful at identifying deep lateral degradation and zones of deep progressive thaw. ERT can identify subsurface massive ice bodies (Herring et al., 2023) and is sensitive to changes in unfrozen-water content that accompanies changing permafrost temperatures. However, ERT is less precise in delineating boundaries, presumably in part due to its sensitivity to unfrozen-water content. ERT measurements and repeat ERT analyses are best confirmed with subsurface boreholes that can be time intensive and difficult to acquire in remote locations. A strength of ERT is it's ability to measure subsurface characteristics to 10s of meters depth but adequate confirmation requires deep boreholes. Both thaw probing and ground-based ERT are time intensive with limited coverage, and require movement across the landscape.

4.2 Degradation and Aggradation Stages

Permafrost thaw can occur along the surface, laterally along the margins, upward along the bottom, and through interior channels. Categorizing degradation and aggradation stages is helpful in assessing permafrost dynamics (Fig. 4). We differentiated five degradation stages that improved our ability to detect permafrost loss. The initial degradation stage differentiates the initial increase in the active layer before talik development. Two of the older burned areas (T1 and TF88) showed increases in initial degradation in response to recent climate warming, while the more recently burned areas (TF01 and TF10) showed decreasing initial degradation with transition rapidly into shallow and deep progressive degradation associated with open talik development. Complete degradation in old thermokarst bogs and fens was widespread across all transects indicating permafrost degradation has been occurring for centuries (Kanevskiy et al. 2014). This differentiation allowed us to distinguish new from old thaw and the increasingly widespread onset of initial thaw.

We found several ages of permafrost that formed in response to climatic change and ecosystem development. At TF10 and T1 some permafrost soils lacked plant macrofossil evidence of previous thermokarst indicating permafrost formed during

https://doi.org/10.5194/egusphere-2024-3997
Preprint. Discussion started: 23 January 2025

the early-mid Holocene (Jorgenson et al., 2001; Brown et al., 2015). At TF88 we found permafrost 23 m thick that had formed low mounds (~0.3 m) in the central portion of an old thermokarst bog, presumably formed during extremely cold winters in the mid-1960s. These mounds disappeared by 2020. At T1 we documented thin (0.1-0.3 m) multi-year frost in soils above shallow taliks and in old thermokarst bogs, mostly during the early 2000s. This sporadic occurrence of multi-year frost greatly complicates the use of mean thaw depths as an overall metric for monitoring permafrost degradation. We presume multi-year frost will no longer form under the warming climate.

4.3 Trends in Lateral versus Vertical Thaw

We found only small changes in the extent of lateral thaw and sharply increasing vertical thaw (initial and progressive degradation combined) from 2012 to 2020, indicating a shift toward widespread vertical thaw and talik development. From 2010 to 2012 the transects had mostly undegraded permafrost on permafrost plateaus and completely degraded permafrost in old thermokarst bogs and fens. By 2020, undegraded permafrost had mostly disappeared.

During colder climate periods, particularly during the Little Ice Age, we think lateral degradation was the primary mechanism for permafrost thaw in boreal regions because of the strong effects of surface and groundwater (Jorgenson et al., 2010; 2022). Recent warming during the last decade, however, has brought near-surface permafrost temperatures close to 0 °C (Smith et al., 2022; Jorgenson et al. in review) and led to recent talik development (Farquharson et al., 2022). In contrast, Jorgenson et al. (2020) found mean lateral degradation rates for permafrost along fens changed little from 1949 to 2018. Furthermore, thermokarst fen and bog expansion in terms of area has been relatively slow: thermokarst fens increased from 3.1% to 4.3% and thermokarst bogs increased from 0.8% to 2.0% from ~1949 to ~2017 (Jorgenson et al. 2020).

4.4 Factors Affecting Degradation and Aggradation

Monitoring of lateral and vertical thaw across four study areas has revealed climate, surface and groundwater, soil characteristics, fire, and vegetation-soil-water interactions all affect rates and patterns of permafrost degradation. Mean annual temperatures in Alaska have increased nearly 2 °C since 1900, with eight of the ten warmest years occurring since 2005 (Walsh et al., 2020). Annual precipitation increased 9% since 1970 with freezing rain events nearly 3 times higher in the 2010s compared to earlier periods (Thoman and Walsh, 2019). Notable extreme precipitation events have occurred in the 2010s and are linked to accelerated permafrost degradation (Douglas et al. 2020). Warmer, snowier winters, which reduce wintertime permafrost cooling, have become more prevalent since 2005 (Jorgenson et al., 2020).

Surface and groundwater temperatures have a large effect on permafrost degradation. Mean annual water temperatures at the bottom of shallow ponds can be 9-11 °C higher than adjacent deep soil and, thus, historically has been a main driver of lateral degradation and thermokarst expansion around lakes and bogs (Jorgenson et al., 2010). Mean annual groundwater temperatures in thermokarst fens (~1. 2 m depth) on the Tanana Flats were frequently near 3 °C, with above freezing

https://doi.org/10.5194/egusphere-2024-3997
Preprint. Discussion started: 23 January 2025

temperatures persisting through winter. All study areas had widespread thermokarst bog coverage with extensive lateral thaw while only two transects (T1 and TF88) had broad thermokarst fen coverage associated with groundwater movement. Transect T1 was unique in having large fens on both sides of a long, narrow permafrost plateau, and had rapid degradation and collapsing birch forests along the portion of the transect adjacent to the fen. This transect had the largest loss of permafrost despite it being unburned.

Soil texture and ground ice contents are highly variable across Tanana Flats (Jorgenson et al., 2001; Brown et al., 2015). This has a large effect on degradation patterns and rates and ability to detect changes. Two of the study areas (T1 and TF88) were relatively ice-rich with thick peat and silts extending down 34 m whereas the other two study areas (TF01 and TF10) had sand and gravel at relatively shallow depths and lower ice contents. The sandier soils and lower ice contents contributed to more rapid thaw and lower thaw settlement. Sand and gravel at depth in fluvial deposits on abandoned floodplains likely contributes to rapid subsurface thawing as groundwater penetrates deeper permafrost. Thus, varying depositional patterns during floodplain development left a legacy of soil and ground ice conditions that can greatly affect permafrost aggradation and degradation (Kreig and Reger 1982; Jorgenson et al. 2022).

Fire can dramatically increase permafrost thaw by removing the vegetation canopy, destroying insulating soil organic material, and changing surface albedo (Brown et al., 2015; Holloway et al., 2020). Differences in soil and hydrology described above confounded our ability to rigorously analyze fire effects. However, large differences among sites allow us to highlight broad effects. First, at the transect with the most recent wildfire (TF10) there was a nearly immediate and rapid increase in shallow progressive degradation following the fire. It was the first time we have observed a fire cause rapid collapse of permafrost terrain to below water level. Second, both of the more recently burned transects (TF01 and TF10) rapidly lost all undegraded permafrost during the early 2010s during a period of substantial climate warming, compared to the older transects (TF88 burned in 1950 and 1988, and T1 unburned since the 1930s) where undegraded permafrost was more persistent. At odds with these trends, the unburned transect T1 also had rapid loss of permafrost due to its proximity to large groundwater fens, and transect TF88, which burned twice, had the largest percentage of undegraded permafrost.

Finally, as permafrost thaws, changes in vegetation, soils, and surface water interact to provide strong feedbacks that affect both permafrost aggradation and degradation. Initially, during collapse of permafrost terrain in flat lowlands, water impounds at the surface providing a positive feedback facilitating further lateral expansion. This lateral degradation was prominent in all study areas. Quickly, however, aquatic sedges, forbs, and mosses colonize the flooded ground and initiate a successional sequence that contributes organic matter for peat accumulation and lifts the surface above water level. These older portions of bogs and fens were prevalent at all transects. At transect TF88 this successional development contributed to the repeated thin permafrost formed within an old bog that was probably initiated during the colder climate of the 1960s. At transect T1, very thin multi-year frost was repeatedly observed in the central old thermokarst bog.

The interactions among climate, hydrology, soils, vegetation, and fire disturbance create a highly patchy mosaic of stable and degrading permafrost. It also makes for a challenging environment to detect permafrost degradation vertically and laterally or where permafrost and thermokarst are of various ages and in differing stages of formation and aggradation. Our monitoring,

https://doi.org/10.5194/egusphere-2024-3997
Preprint. Discussion started: 23 January 2025

however, came at a time of recent substantial increased temperatures and precipitation, and we believe we have detected a large shift from past narrower and slower lateral degradation to more rapid and widespread vertical degradation. Given the positive and negative aspects of ground surface surveys, airborne lidar, and geophysical investigations a coupled application of these methods is warranted to track permafrost thaw. Future applications of these methods should apply geospatial analyses and machine learning to identify variables relating surface and subsurface conditions to project finer scale field-based spatial assessments across broader regions.

5. Conclusions

It is clear from our repeat ground surface surveys that interior Alaska permafrost is undergoing widespread and dramatic thaw degradation. Between 2004 and 2020 top-down thaw of near surface permafrost doubled from 18% to 36%. Multi-year frost and repeat thin permafrost, two types of permafrost aggradation, were almost completely absent by 2020. To better assess these changes in permafrost at our sites we differentiated degradation stages with an emphasis on contrasting vertical versus lateral thaw. Shallow and deep progressive degradation (i.e. top-down thaw of near surface permafrost) increased from 18% to 36% across our study sites over the 8 year study period. Lateral thaw of tabular shaped permafrost boundaries and development of unfrozen zones between the bottom of the seasonally frozen layer and the top of near-surface permafrost (taliks) were evident, supporting recent identification of widespread talik development across the region (Farquharson et al., 2022). Repeat airborne Lidar also identified lateral and vertical loss of near-surface permafrost at all of our sites with 60% of the area at one field site exhibiting vertical thaw. Much of the permafrost thaw at our sites is associated with the press disturbance of climate warming. However, rapid loss of near-surface permafrost was initiated immediately after the pulse disturbance of the 2010 fire with subsidence of up to 1 m in the subsequent decade.

There are numerous approaches for assessing permafrost changes, including thaw probing (Nelson et al., 2021; Douglas et al., 2020), temperature monitoring (Farquharson et al., 2022), ERT (Douglas et al., 2016; Minsley et al., 2022; Herring et al., 2023), Lidar measurements (Douglas et al., 2022), photogrammetry (Van der Sluijs et al., 2018), and synthetic aperture radar (Zweiback and Meyer, 2021), and remote sensing of thermokarst landforms (Jorgenson et al., 2016, Kokelj et al., 2020). We used results from repeated thaw probe measurements, ERT, and airborne Lidar to assess their relative strengths and weaknesses for quantifying changes in ecosystem-driven discontinuous permafrost in a boreal ecosystem. Across all methods we found monitoring boreal permafrost is challenging because the three-dimensional nature of permafrost bodies makes them sensitive to climate, hydrology, water-soil-vegetation interactions, and fire disturbance. Future applications of these methods should apply geospatial analyses to identify variables relating surface and subsurface conditions to project finer scale field-based spatial assessments across broader regions.

Data availability statement

The data that support the findings of this study are available upon reasonable request from the authors.

https://doi.org/10.5194/egusphere-2024-3997
Preprint. Discussion started: 23 January 2025

Author Contribution

TAD oversaw study activities. MTJ designed and led field measurements. TDS applied geophysical methods and analyses. CZ developed and applied geospatial analyses of thaw and generated map products. All authors contributed to data analysis and manuscript preparation.

Competing Interests

The authors declare that they have no conflict of interest.

Acknowledgements

We appreciate the efforts of numerous amazing scientists and engineers that participated in field measurements over the years.

Financial Support

This research was funded by the Department of Defense's Strategic Environmental Research and Development Program (Project RC18- 1170) and Environmental Science and Technology Certification Program (Project RC22-D3-7408) as well as the U.S. Army Engineer Research and Development Center Basic Research Portfolio through Program Element 0601102A/T14/ST1409.

ORCID iD

Thomas A Douglas https://orcid.org/0000-0003-1314-1905

References

Blanchy, G., Saneiyan, S., Boyd, J., McLachlan, P., & Binley, A. (2020). ResIPy, an intuitive open source software for complex geoelectrical inversion/modeling. Computers & Geosciences, 137, 104423.

Brodylo D, Douglas TA, Zhang C. Quantification of active layer depth at multiple scales in interior Alaska permafrost. Environmental Research Letters. 2024 Feb 16;19(3):034013.

https://doi.org/10.5194/egusphere-2024-3997
Preprint. Discussion started: 23 January 2025

Brown DR, Jorgenson MT, Douglas TA, Romanovsky VE, Kielland K, Hiemstra C, Euskirchen ES, Ruess RW. Interactive effects of wildfire and climate on permafrost degradation in Alaskan lowland forests. Journal of Geophysical Research: Biogeosciences. 2015 Aug;120(8):1619-37.

Buckel J, Mudler J, Gardeweg R, Hauck C, Hilbich C, Frauenfelder R, Kneisel C, Buchelt S, Blöthe JH, Hördt A, Bücker M. Identifying mountain permafrost degradation by repeating historical ERT-measurements. The Cryosphere Discussions. 2022 Nov 23;2022:1-36.

Chacho, E., S. Arcone, and A. Delaney, 1995, Blair Lakes target facility permafrost and groundwater study: U.S. Army Cold Regions Research and Engineering Laboratory, Technical report, 30.

Dagenais S, Molson J, Lemieux JM, Fortier R, Therrien R. Coupled cryo-hydrogeological modelling of permafrost dynamics near Umiujaq (Nunavik, Canada). Hydrogeology Journal. 2020 May 1;28(3):887-904.

Douglas TA, Jones MC, Hiemstra CA, Arnold JR. Sources and sinks of carbon in boreal ecosystems of interior Alaska: A review. Elementa: Science of the Anthropocene. 2014 Jan 1;2.

Douglas TA, Jorgenson MT, Brown DR, Campbell SW, Hiemstra CA, Saari SP, Bjella K, Liljedahl AK. Degrading permafrost mapped with electrical resistivity tomography, airborne imagery and lidar, and seasonal thaw measurements. Geophysics. 2016 Jan 1;81(1):WA71-85.

Douglas TA, Hiemstra CA, Jones MC, Arnold JR. Sources and sinks of carbon in boreal ecosystems of interior Alaska: A review.

Douglas TA, Hiemstra CA, Anderson JE, Barbato RA, Bjella KL, Deeb EJ, Gelvin AB, Nelsen PE, Newman SD, Saari SP, Wagner AM. Recent degradation of interior Alaska permafrost mapped with ground surveys, geophysics, deep drilling, and repeat airborne lidar. The Cryosphere. 2021 Aug 3;15(8):3555-75.

Douglas, T.A., Barker, A.J., Monteith, A.J., Froese, D.G. Development of a Local Meteoric Water Line for interior Alaska Used to Calculate Paleoclimate Conditions From Permafrost Representing the past 40,000 Years. In review.

Euskirchen ES, Edgar CW, Kane ES, Waldrop MP, Neumann RB, Manies KL, Douglas TA, Dieleman C, Jones MC, Turetsky MR. Persistent net release of carbon dioxide and methane from an Alaskan lowland boreal peatland complex. Global Change Biology. 2024 Jan;30(1):e17139.

Farquharson LM, Romanovsky VE, Kholodov A, Nicolsky D. Sub-aerial talik formation observed across the discontinuous permafrost zone of Alaska. Nature Geoscience. 2022 Jun;15(6):475-81.

Foster AC, Armstrong AH, Shuman JK, Shugart HH, Rogers BM, Mack MC, Goetz SJ, Ranson KJ. Importance of tree-and species-level interactions with wildfire, climate, and soils in interior Alaska: Implications for forest change under a warming climate. Ecological Modelling. 2019 Oct 1;409:108765.

Gibson CM, Chasmer LE, Thompson DK, Quinton WL, Flannigan MD, Olefeldt D. Wildfire as a major driver of recent permafrost thaw in boreal peatlands. Nature communications. 2018 Aug 2;9(1):3041.

https://doi.org/10.5194/egusphere-2024-3997
Preprint. Discussion started: 23 January 2025

Herring T, Lewkowicz AG, Hauck C, Hilbich C, Mollaret C, Oldenborger GA, Uhlemann S, Farzamian M, Calmels F, Scandroglio R. Best practices for using electrical resistivity tomography to investigate permafrost. Permafrost and Periglacial Processes. 2023 Oct;34(4):494-512.

Hjort J, Streletskiy D, Doré G, Wu Q, Bjella K, Luoto M. Impacts of permafrost degradation on infrastructure. Nature Reviews Earth & Environment. 2022 Jan;3(1):24-38.

Holloway JE, Lewkowicz AG, Douglas TA, Li X, Turetsky MR, Baltzer JL, Jin H. Impact of wildfire on permafrost landscapes: A review of recent advances and future prospects. Permafrost and Periglacial Processes. 2020 Jul;31(3):371-82.

Johnstone JF, Celis G, Chapin III FS, Hollingsworth TN, Jean M, Mack MC. Factors shaping alternate successional trajectories in burned black spruce forests of Alaska. Ecosphere. 2020 May;11(5):e03129.

Jones BM, Stoker JM, Gibbs AE, Grosse G, Romanovsky VE, Douglas TA, Kinsman NE, Richmond BM. Quantifying landscape change in an arctic coastal lowland using repeat airborne lidar. Environmental Research Letters. 2013 Nov 21;8(4):045025.

Jones MC, Booth RK, Yu Z, Ferry P. A 2200-year record of permafrost dynamics and carbon cycling in a collapse-scar bog, interior Alaska. Ecosystems. 2013 Jan;16:1-9.

Jorgenson MT, Roth JE, Raynolds MK, Smith MD, Lentz W, Zusi-Cobb, A.L., Racine, C.H. (1999) An Ecological Land Survey for Fort Wainwright, Alaska. CRREL REPORT 99-9, 92 pages.

Jorgenson MT, Racine CH, Walters JC, Osterkamp TE. Permafrost degradation and ecological changes associated with a warming climate in central Alaska. Climatic change. 2001 Mar;48(4):551-79.

Jorgenson MT, Romanovsky V, Harden J, Shur Y, O'Donnell J, Schuur EA, Kanevskiy M, Marchenko S. Resilience and vulnerability of permafrost to climate change. Canadian Journal of Forest Research. 2010 Jul;40(7):1219-36.

Jorgenson, M. T., M. Kanevskiy, Y. Shur, T. Osterkamp, D. Fortier, T. Cater, and P. Miller, 2012, Thermokarst lake and Shore Fen development in boreal Alaska, in K. Hinkel, ed., Proceedings of the Tenth International Conference on Permafrost, University of Alaska Fairbanks; 179–184.

Jorgenson MT, Grosse G. Remote sensing of landscape change in permafrost regions. Permafrost and periglacial processes. 2016 Oct;27(4):324-38.

Jorgenson MT, Douglas TA, Liljedahl AK, Roth JE, Cater TC, Davis WA, Frost GV, Miller PF, Racine CH. The roles of climate extremes, ecological succession, and hydrology in repeated permafrost aggradation and degradation in fens on the Tanana Flats, Alaska. Journal of Geophysical Research: Biogeosciences. 2020 Dec;125(12):e2020JG005824.

Jorgenson MT, Brown DR, Hiemstra CA, Genet H, Marcot BG, Murphy RJ, Douglas TA. Drivers of historical and projected changes in diverse boreal ecosystems: fires, thermokarst, riverine dynamics, and humans. Environmental Research Letters. 2022 Mar 25;17(4):045016.

Jorgenson MT, Douglas TA, Kanevskiy, M., Shur, Y. (in review) Mapping the Vulnerability of Boreal Permafrost in Relation to Thaw Rate, Ground Ice, and Thermokarst Transitions. Earth Surface Processes.

https://doi.org/10.5194/egusphere-2024-3997
Preprint. Discussion started: 23 January 2025

Kanevskiy M, Jorgenson T, Shur Y, O'Donnell JA, Harden JW, Zhuang Q, Fortier D. Cryostratigraphy and permafrost evolution in the lacustrine lowlands of west-Central Alaska. Permafrost and Periglacial Processes. 2014 Jan;25(1):14-34.

Kokelj SV, Kokoszka J, van der Sluijs J, Rudy AC, Tunnicliffe J, Shakil S, Tank S, Zolkos S. Permafrost thaw couples slopes with downstream systems and effects propagate through Arctic drainage networks. The Cryosphere Discussions. 2020 Sep 28;2020:1-43.

Kreig, R. A. and Reger, R. D.: 1982, Air-Photo Analysis and Summary of Landform Soil Properties along the Route of the Trans-Alaska Pipeline System, Alaska Division of Geological and Geophysical Surveys, Fairbanks, AK, Geol. Rep. 66, 149.

Lara MJ, Genet H, McGuire AD, Euskirchen ES, Zhang Y, Brown DR, Jorgenson MT, Romanovsky V, Breen A, Bolton WR. Thermokarst rates intensify due to climate change and forest fragmentation in an Alaskan boreal forest lowland. Global Change Biology. 2016 Feb;22(2):816-29.

Lewkowicz AG, Etzelmüller B, Smith SL. Characteristics of discontinuous permafrost based on ground temperature measurements and electrical resistivity tomography, southern Yukon, Canada. Permafrost and periglacial processes. 2011 Oct;22(4):320-42.

Liston GE, Hiemstra CA. The changing cryosphere: Pan-Arctic snow trends (1979–2009). Journal of Climate. 2011 Nov 1;24(21):5691-712.

Marshall AM, Link TE, Flerchinger GN, Lucash MS. Importance of parameter and climate data uncertainty for future changes in boreal hydrology. Water Resources Research. 2021 Aug;57(8):e2021WR029911.

McNeill D, Hoekstra P. In-situ measurements on the conductivity and surface impedance of sea ice at VLF. Radio Science. 1973 Jan;8(1):23-30.

Mekonnen ZA, Riley WJ, Randerson JT, Grant RF, Rogers BM. Expansion of high-latitude deciduous forests driven by interactions between climate warming and fire. Nature plants. 2019 Sep;5(9):952-8.

Mewes B, Hilbich C, Delaloye R, Hauck C. Resolution capacity of geophysical monitoring regarding permafrost degradation induced by hydrological processes. The Cryosphere. 2017 Dec 14;11(6):2957-74.

Minsley B, Wellman TP, Walvoord MA, Revil A. Sensitivity of airborne geophysical data to sublacustrine and near-surface permafrost thaw. Cryosphere. 2015 Mar 1;9(2).

Minsley BJ, Pastick NJ, James SR, Brown DR, Wylie BK, Kass MA, Romanovsky VE. Rapid and gradual permafrost thaw: A tale of two sites. Geophysical Research Letters. 2022 Nov 16;49(21):e2022GL100285.

Nelson FE, Shiklomanov NI, Nyland KE. Cool, CALM, collected: the Circumpolar Active Layer Monitoring program and network. Polar Geography. 2021 Jul 3;44(3):155-66.

O'Donnell, J. A., M. T. Jorgenson, J. W. Harden, A. D. McGuire, M. Z. Kanevskiy, and K. P. Wickland, 2012, The effects of permafrost thaw on soil hydrologic, thermal, and carbon dynamics in an Alaskan peatland: Ecosystems, 15, 213–229, doi: 10.1007/s10021-011-9504-0.

Osterkamp TE. The recent warming of permafrost in Alaska. Global and Planetary Change. 2005 Dec 1;49(3-4):187-202.

https://doi.org/10.5194/egusphere-2024-3997
Preprint. Discussion started: 23 January 2025

Potter C, Hugny C. Wildfire effects on permafrost and soil moisture in spruce forests of interior Alaska. Journal of forestry research. 2020 Apr;31(2):553-63.

Shur YL, Jorgenson MT. Patterns of permafrost formation and degradation in relation to climate and ecosystems. Permafrost and Periglacial Processes. 2007 Jan;18(1):7-19.

Smith SL, O'Neill HB, Isaksen K, Noetzli J, Romanovsky VE. The changing thermal state of permafrost. Nature Reviews Earth & Environment. 2022 Jan;3(1):10-23.

Thoman R, Walsh JE. Alaska's Changing Environment: documenting Alaska's physical and biological changes through observations. International Arctic Research Center, University of Alaska Fairbanks; 2019.

Uhlemann S, Dafflon B, Peterson J, Ulrich C, Shirley I, Michail S, Hubbard SS. Geophysical monitoring shows that spatial heterogeneity in thermohydrological dynamics reshapes a transitional permafrost system. Geophysical Research Letters. 2021 Mar 28;48(6):e2020GL091149.

Van der Sluijs J, Kokelj SV, Fraser RH, Tunnicliffe J, Lacelle D. Permafrost terrain dynamics and infrastructure impacts revealed by UAV photogrammetry and thermal imaging. Remote Sensing. 2018 Nov 3;10(11):1734.

Walsh JE, Ballinger TJ, Euskirchen ES, Hanna E, Mård J, Overland JE, Tangen H, Vihma T. Extreme weather and climate events in northern areas: A review. Earth-Science Reviews. 2020 Oct 1;209:103324.

Wolken JM, Hollingsworth TN, Rupp TS, Chapin III FS, Trainor SF, Barrett TM, Sullivan PF, McGuire AD, Euskirchen ES, Hennon PE, Beever EA. Evidence and implications of recent and projected climate change in Alaska's forest ecosystems. Ecosphere. 2011 Nov;2(11):1-35.

Zhang C, Douglas TA, Anderson JE. Modeling and mapping permafrost active layer thickness using field measurements and remote sensing techniques. International Journal of Applied Earth Observation and Geoinformation. 2021 Oct 1;102:102455.

Zhang C, Douglas TA, Brodylo D, Jorgenson MT. Linking repeat lidar with Landsat products for large scale quantification of fire-induced permafrost thaw settlement in interior Alaska. Environmental Research Letters. 2023 Jan 3;18(1):015003.

Zhang C, Douglas TA, Brodylo D, Bosche LV, Jorgenson MT. Combining a climate-permafrost model with fine resolution remote sensor products to quantify active-layer thickness at local scales. Environmental Research Letters. 2024 Mar 19;19(4):044030.

Zwieback S, Meyer FJ. Top-of-permafrost ground ice indicated by remotely sensed late-season subsidence. The Cryosphere. 2021 Apr 23;15(4):2041-55.